

A COMPARISON OF EXTENDED KALMAN FILTER APPROACHES USING NON-LINEAR TEMPERATURE AND ULTRASOUND TIME-OF-FLIGHT MEASUREMENT MODELS FOR HEATING SOURCE LOCALIZATION OF A TRANSIENT HEAT TRANSFER PROBLEM

Michael R. Myers

*Dept. of Mechanical Engineering
Vanderbilt University
Nashville, Tennessee, U.S.A.
mike.myers@vanderbilt.edu*

Ariosto B. Jorge

*Mechanical Engineering Institute
Federal University of Itajubá
Itajubá, MG, Brazil
ariosto.b.jorge@unifei.edu.br*

D. Greg Walker

*Dept. of Mechanical Engineering
Vanderbilt University
Nashville, Tennessee, U.S.A.
greg.walker@vanderbilt.edu*

ABSTRACT

State estimation procedures using the extended Kalman filter are investigated for a transient heat transfer problem in which a heat source is applied on one side of a thin plate and ultrasonic time of flight or temperature is measured on the other side of the plate. A forward conduction solution is developed using finite element methods and verified using closed-form analytic solutions and validated using thermal conduction experiments. Parameter identification of experiment heating source magnitude and convection coefficient is conducted with least squares, extended Kalman filter, and extended information filter. Comparisons of six heating source localization measurement models are conducted where temperature or ultrasonic time of flight readings provide the measurement update to the extended Kalman filter. For each quantity of interest being investigated, two different measurement models are implemented: 1) directly using the quantity of interest at the sensor locations as the measurement vector and 2) indirectly obtaining distance from the quantity of interest and then using these obtained distances as the measurement vector in the extended Kalman filter. For the direct models, the Jacobian required by the extended Kalman filter is obtained numerically using finite differences from the finite element forward conduction solution. For the indirect models, the derivatives of the distances with respect to the state variables are obtained in closed form. Heating source localization results and convergence behavior are compared for the six measurement models

investigated.

NOMENCLATURE

α	thermal diffusivity (m^2/s)
C_p	specific heat ($\text{J}/\text{kg K}$)
E	Young's modulus (GPa)
G	ultrasonic time of flight (s)
h	convection heat transfer coefficient ($\text{W}/\text{m}^2 \text{K}$)
k	thermal conductivity (kg/m^3)
L	length (m)
q''	heat flux (W/m^2)
T	temperature ($^\circ\text{C}$)
t	time (s)
v	sound speed (m/s)
θ	temperature change relative to reference (K)
ξ	ultrasonic time of flight temperature factor ($1/\text{K}$)
ρ	density (kg/m^3)

INTRODUCTION

Knowledge of where air flowing across a body transitions from laminar flow to turbulent flow can provide numerous benefits to air vehicle design, thermal protection system design, and air vehicle in-flight control [1]. At the transition between these two flow regimes, a change in body-surface temperature has been measured [2]. The objective of this and follow-on work is to develop a method to locate and characterize the heat flux change induced by the boundary layer transition. The solution involves a forward conduction solution and an inverse procedure. The work presented here

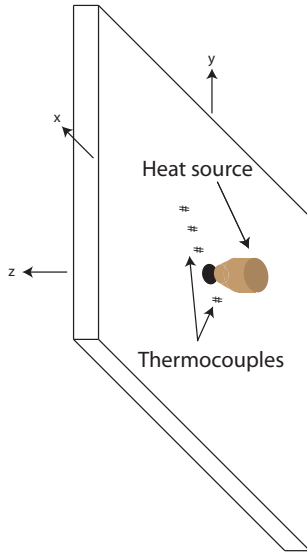


Figure 1. Illustration of flat plate with heat source and sensors (not drawn to scale).

focuses on forward conduction solution, flat plate experimentation with a known heat source, parameter identification of the applied heat flux and the convection coefficient, and comparing six measurement models for heating source localization.

FORWARD CONDUCTION SOLUTION

This work focuses first on a large flat plate heated over a small area with a known heat source. Consider a 61cm x 30.5cm x 0.635cm stainless steel 316L plate with constant properties of $k = 15 \text{ W/m K}$, $C_p = 500 \text{ J/kg K}$ and $\rho = 8,000 \text{ kg/m}^3$ (Figure 1). The heating source is fixed at the plate center, is applied at $t = 300 \text{ sec}$ and removed at $t = 600 \text{ sec}$, and has a heating profile of $q = 1.7 \text{ MW/m}^2$ over 0.635 cm diameter circular area. Radiation effects are assumed to be negligible.

The forward conduction solution leverages COMSOL Multiphysics by the COMSOL Group and uses a finite element mesh with smaller elements near the heat source and larger elements near the plate edges to conserve computing resources. A grid convergence study was performed to ensure grid independence. Both the number of elements in the plate's x-y plane and the number of layers in the plate's thickness were considered. Figure 2

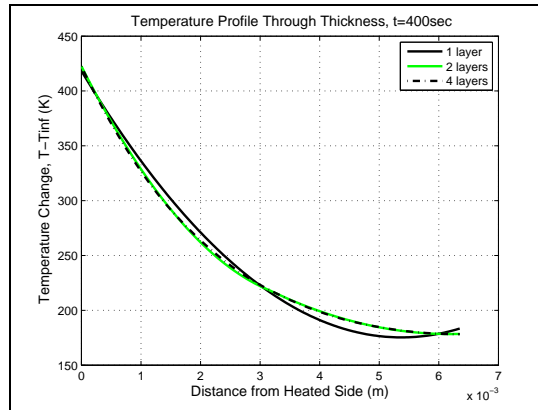


Figure 2. Number of mesh layers for best accuracy.

illustrates the results of this study for the number of layers. The grid convergence study led to the selection of three mesh layers through the plate's thickness dimension, 9,780 total elements, and 45,983 degrees of freedom. Independent verification of the numerical solution was performed using a closed-form, analytical solution of heating through a circular domain without convection [3]. Agreement between the COMSOL solution and the closed-form solution is acceptable with mean absolute error less than 0.5 K.

FLAT PLATE EXPERIMENT

Eight K-type thermocouples were attached to a 61cm x 30.5cm x 0.635cm plate of stainless steel 316L. The plate was sized such that the plate edges would not affect the temperature profile in the plate during the experiment. Four thermocouples were attached on one side and four on the other. With plate center being the origin and the x-axis being the length (Figure 1), thermocouples were attached at (x, y) locations of (1cm, 1cm), (2cm, 2cm), (3cm, 3cm), and (-1cm, -1cm) on the heated side ($z = 0$) and on the non-heated side ($z=0.635\text{cm}$). The desire was to have thermocouple pairs in exactly the same position on either side of the plate allowing measurement of the temperature difference between the two sides. The thermocouples were secured to the plate with thermal grease and Kapton tape to ensure good thermal contact. Flat black paint was applied to a 1.5 cm diameter area

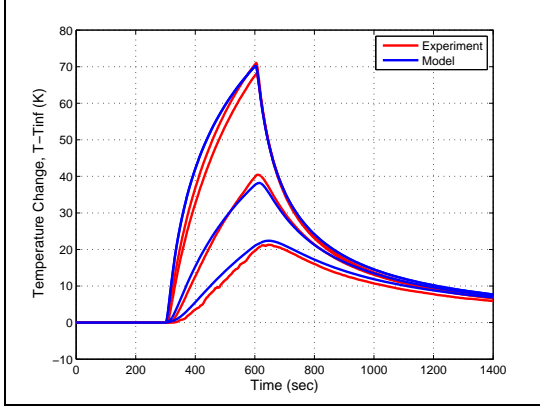


Figure 3. Temperature response on non-heated side of the plate at four sensor locations.

at the plate center to maximize energy absorption from the heater. The plate was oriented vertically with the positive y -axis pointing up. A Research, Inc. SpotIR 4150 heater with focusing cone was positioned approximately 2mm from the plate surface such that its beam struck the plate center. Experiments were conducted with the heater running at full-power which, according to manufacturer's specifications, produces 1.7 MW/m^2 of heat flux on the plate in a circular area 0.635 cm in diameter. Consequently, approximately 54 Watts of energy are being absorbed by the plate when the heater is on.

During the experiment, the heater is turned on at $t = 300$ seconds and turned off and removed at $t = 600$ seconds. Data acquisition equipment was used to record thermocouple temperature readings every second during the experiment. A MIKRON Thermo Scan TS7302 infrared camera was used to collect thermal images of the plate and heater. Coupled with a laptop computer, this system recorded thermal images every five seconds during the experiment. Figure 3 illustrates the temperature data recorded during the experiment. Discrepancies between the two thermocouple sets closest to the source [(1cm, 1cm) and (-1cm, -1cm)] arise from sensor placement error.

PARAMETER IDENTIFICATION

Even with manufacturer specifications, the heat transfer between the radiative heater and the plate is not known with much certainty. Further complicating matters, the heater's proximity to the plate implies an unknown amount of secondary radiation and convection heating on the plate. The focusing cone reaches temperatures in excess of 200°C and the lamp is cooled with forced air that exits the heater through the focusing cone pointed at the plate. For this initial analysis, the main heat flux and convection coefficient are estimated. The secondary heating is modeled with a Gaussian profile of $q_g'' = 100 \text{ W/m}^2$ and $\sigma_g^2 = 0.0009 \text{ m}^2$. The heat transfer coefficient h is assumed constant and identical on both sides of the plate. Estimating h using free convection correlations [4] produces an expected range of $2 \text{ W/m}^2\text{K} \leq h \leq 5 \text{ W/m}^2\text{K}$. Since the plate edges do not contribute significantly to the thermal load, $h = 3 \text{ W/m}^2\text{K}$ is assumed on all four plate edges.

Three inverse methods are compared to quantify the heat flux (q) and convection coefficient (h) on the plate: least squares, extended Kalman filter, and extended information filter. The extended Kalman filter and extended information filter are members of a family of recursive state estimators, collectively called Gaussian filters [5]. The extended information filter is the information form of the Kalman filter. Both filters linearize nonlinear Gaussian systems. For the inversion, the entire experiment is treated as one event, and all temperature measurements are combined together. The 5,056 temperature measurements therefore are effectively 5,056 separate sensors. All three methods start with an initial guess of the state $x_0 = [q \ h]^T = [1.7 \text{ MW/m}^2 \ 5.0 \text{ W/m}^2\text{K}]^T$ and are processed recursively to convergence.

The least squares estimator is $x_{new} = x + (X_\beta^T X_\beta)^{-1} X_\beta^T (Y - T|_x)$ where X is the Jacobian based on finite differences obtained by independently varying the state parameters 0.1%, Y are the experimentally obtained temperatures, and $T|_x$ are temperatures based on current estimates for the state x [6]. The Jacobian was normalized to produce a better conditioned matrix. The algorithm for the extended Kalman filter is listed in Table 1 where \bar{X}_t is the predicted state, $a(U_t, X_{t-1})$

is the state model based on the input U_t and the previous state X_{t-1} , A is the state Jacobian, $\bar{\Sigma}$ is the uncertainty estimate, Q_t is the state covariance, K_t is the Kalman gain, B_t is the measurement Jacobian, R_t is the measurement covariance, $b(\bar{X}_t)$ is the measurement transition function and represents the predicted measurements from the forward conduction solution based on the predicted state, and Z_t represents the actual measurements. The filter represents the belief at time t by the state X_t and the covariance Σ_t . For the flat plate considered here, there is no input to the state thus the state model is $a = I_2$ and the state Jacobian is $A = I_2$, where I_2 is a 2×2 identity matrix. The measurement transition function b is a $5,056 \times 1$ matrix of the predicted temperatures from the forward conduction solution, and the measurement Jacobian B is obtained using finite differences (a $5,056 \times 2$ matrix) by independently varying the state parameters 0.1%. The state covariance matrix Q is a 2×2 diagonal matrix using $\sigma_q^2 = 0.1 \text{ MW}^2/\text{m}^4$ and $\sigma_h^2 = 0.1 \text{ W}^2/\text{m}^4\text{K}^2$. These values were chosen to achieve smooth convergence behavior since small values for the state covariance matrix cause the Gaussian filters to diverge while arbitrarily large values for the state covariance matrix render the Gaussian filters essentially identical to the least squares method. The thermocouples have a measurement accuracy of $\pm 1.5^\circ\text{C}$, which translates to a measurement variance of $\sigma_T^2 = 0.25^\circ\text{C}^2$. This value was used for the diagonal elements of the measurement covariance matrix R , a $5,056 \times 5,056$ matrix. The filter is initialized with the initial state x_0 (stated above) and covariance $\Sigma_0 = 0$. For the extended information filter (Table 2), a , A , b , B , R , and Q are identical to those in the extended Kalman filter. The extended information filter possesses an advantage of allowing the inverse of the measurement covariance matrix Q^{-1} to be computed once and reused for all iterations. Because the initial state covariance matrix Σ_0 is inverted in the extended information filter, the filter was initialized with $\Sigma_0 = R$ instead of the zero matrix used to initialize the extended Kalman filter.

Figures 4 and 5 illustrate the convergence behavior for all three methods. The extended Kalman filter and extended information filter converge identically and are presented together. The Gaussian

Table 1. Extended Kalman filter algorithm.

Step	Operation
1	$\bar{X}_t = a(U_t, X_{t-1})$
2	$\bar{\Sigma}_t = A_t \Sigma_{t-1} A_t^T + Q_t$
3	$K_t = \bar{\Sigma}_t B_t^T (B_t \bar{\Sigma}_t B_t^T + R_t)^{-1}$
4	$X_t = \bar{X}_t + K_t (Z_t - b(\bar{X}_t))$
5	$\Sigma_t = (I - K_t B_t) \bar{\Sigma}_t$
6	Return to step 1 if solution not converged

Table 2. Extended information filter algorithm.

Step	Operation
1	$X_{t-1} = \Omega_{t-1}^{-1} \phi_{t-1}$
2	$\bar{\Omega}_t = (A \Omega_{t-1}^{-1} A^T + Q)^{-1}$
3	$\bar{\phi}_t = \bar{\Omega}_t a(U_t, X_{t-1})$
4	$\bar{X}_t = a(U_t, X_{t-1})$
5	$\Omega_t = \bar{\Omega}_t + B^T R^{-1} B$
6	$\phi_t = \bar{\phi}_t + B R^{-1} [Z_t - b(\bar{X}_t) + B \bar{X}_t]$
7	Return to step 1 if solution not converged

filters converge a bit slower than the least squares method, however the convergence is smoother. Once convergence was achieved, statistical moments were computed from the last three iterations. Results are similar for all three methods. Computational cost is lowest with least squares, followed by extended information filter, and then extended Kalman filter. Figure 3 compares the temperature response measured during the experiment with the temperature response of the model using $q = 0.930 \text{ MW}/\text{m}^2$ and $h = 3.20 \text{ W}/\text{m}^2\text{K}$. Agreement between the model and the experiment is acceptable, however improvement could be achieved through modifications to the heating profile (e.g., secondary heating). A check of the boundary effect errors was conducted to ensure the plate was sized sufficiently large. Of particular interest is in the region of $(\pm 4\text{cm}, \pm 4\text{cm})$ where the errors remain well below 0.5% for the entire experiment. Even at $(\pm 10\text{cm}, \pm 10\text{cm})$, the errors are below 1% for much of the experiment and stay below 3% for

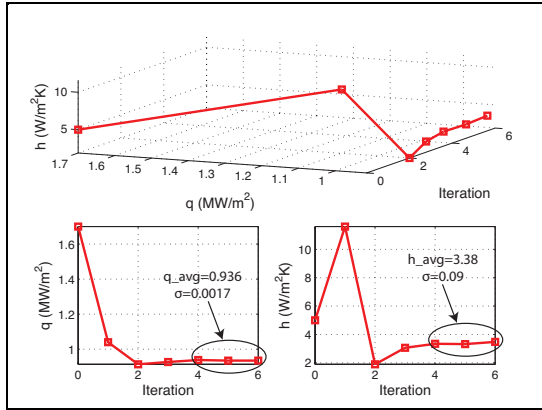


Figure 4. Least squares convergence.

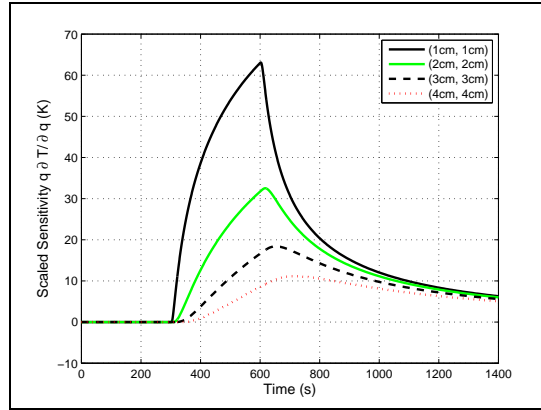


Figure 6. Heat flux sensitivity.

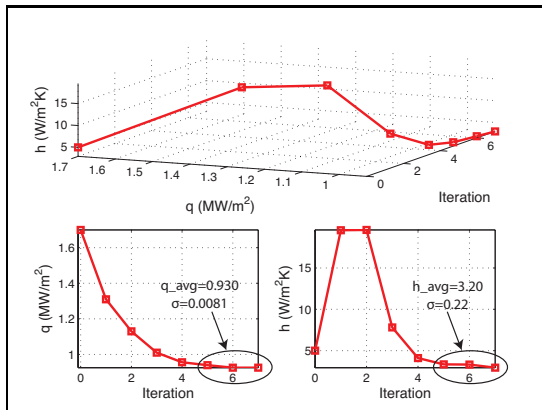


Figure 5. Extended Kalman filter and extended information filter convergence. The filters produce identical results and are presented together.

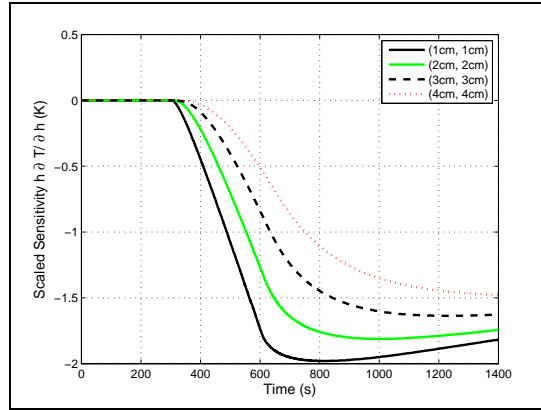


Figure 7. Convection coefficient sensitivity.

the entire experiment. Solution sensitivity analysis was performed to find $q\partial T/\partial q$ and $h\partial T/\partial h$ versus time using finite differences (Figures 6 and 7). These figures indicate q and h are not correlated and q dominates the solution.

HEATING SOURCE LOCALIZATION

Locating and characterizing a heating source depends upon many factors such as heating source movements in time, heating source magnitude changes in time, and other transient behaviors. Fairly restrictive assumptions can be imposed that simplify

the problem. Analysis and algorithm development can proceed using these restrictive assumptions and then assumptions can be relaxed in stages to achieve the end result of source localization and characterization. The assumptions for this work are:

1. Source in fixed position (location unknown)
2. Source applied at time $t = 300$ sec and removed at $t = 600$ sec
3. $q = 0.930$ MW/m² over 0.00635 m diameter circular area while source applied (value obtained in parameter identification above)
4. Secondary heating is characterized by a Gaussian with magnitude $q_g = 100$ W/m² and

variance $\sigma_g^2 = 0.0009 \text{ m}^2$ while source applied

5. Convection coefficient $h = 3.20 \text{ W/m}^2\text{K}$ on both sides of the plate (value obtained in parameter identification above)
6. Convection coefficient $h = 3 \text{ W/m}^2\text{K}$ on the plate edges
7. Thermal conductivity $k = 15 \text{ W/mK}$
8. Specific heat $C_p = 500 \text{ J/kgK}$ and density $\rho = 8,000 \text{ kg/m}^3$
9. Positions of sensors are $(\pm 4\text{cm}, \pm 4\text{cm})$ on the non-heated side

The following six measurement models have been identified for analysis:

1. Temperature measurement model
2. Radius from temperature measurement model
3. Ultrasonic pulse-echo time of flight measurement model
4. Radius from ultrasonic pulse-echo time of flight measurement model
5. Ultrasonic pulse one-way time of flight measurement model
6. Ellipse from ultrasonic one-way pulse time of flight measurement model

These measurement models represent different ways to collect measurements (sensors) and different ways to process the data. Two measurement models are based on thermocouple sensors and four models are based on ultrasonic transducer sensors. Comparison of the six measurement models is performed using the extended Kalman filter (algorithm in Table 1) to locate the source (x_q, y_q) . For all six measurement models, the state is $X_t = [x_q, y_q]^T$ and there is no input to the state thus the state model is $a = I_2$, the state Jacobian is $A = I_2$. Sensitivity of the state variance was compared for values from $\sigma^2 = 0.01 \text{ m}^2$ to 0.000001 m^2 with the lower values providing a damping effect. A state variance of $\sigma^2 = 0.0001 \text{ m}^2$ provides a good compromise between damping and stability and will be used for all measurement model comparisons in this work. Thus, the state covariance matrix is $Q_t = 0.0001 \text{ m}^2 * I_2$, where I_2 is a 2×2 identity matrix.

Temperature Measurement Model

In this model, temperatures are measured using four thermocouples on the non-heated side of the plate. Expected temperatures and the partial derivatives are obtained directly from COMSOL to form the measurement transition function $b(\bar{X}_t)$ and the Jacobian B_t .

$$b(\bar{X}_t) = \begin{bmatrix} \bar{\theta}_1 \\ \bar{\theta}_2 \\ \bar{\theta}_3 \\ \bar{\theta}_4 \end{bmatrix} \quad (1)$$

$$B_t = \begin{bmatrix} -\frac{\partial \bar{\theta}_1}{\partial x_1} & -\frac{\partial \bar{\theta}_1}{\partial y_1} \\ -\frac{\partial \bar{\theta}_2}{\partial x_2} & -\frac{\partial \bar{\theta}_2}{\partial y_2} \\ -\frac{\partial \bar{\theta}_3}{\partial x_3} & -\frac{\partial \bar{\theta}_3}{\partial y_3} \\ -\frac{\partial \bar{\theta}_4}{\partial x_4} & -\frac{\partial \bar{\theta}_4}{\partial y_4} \end{bmatrix} \quad (2)$$

where t is time in seconds with a time step of 1 second, $\bar{\theta}$ is the change in temperature relative to a reference if the heating source is located at (x_s, y_s) , and (x_i, y_i) with $i = 1, 2, 3, 4$ are the locations of the four thermocouples. The Jacobian B_t is constructed using the derivatives with respect to sensor position for convenience since this information can be obtained with one COMSOL simulation. The derivatives are obtained directly from COMSOL. Based on the flat plate experiment above, sensor noise is assumed be $\pm 0.045 \text{ K}$ and is normally distributed ($\sigma^2 = (0.045/3)^2 = 2.225 \times 10^{-4} \text{ K}^2$). The measurement covariance matrix is $R = 2.225 \times 10^{-4} \text{ K}^2 * I_4$.

Radius From Temperature Measurement Model

This model is similar to the previous model in that temperatures are measured using thermocouples. While temperatures are measured with the thermocouples, COMSOL is used as a lookup table to convert temperatures to a radius from each sensor to the source.

$$r_i = \sqrt{(x_i - x_s)^2 + (y_i - y_s)^2} \quad (3)$$

where (x_i, y_i) is the location of sensor i for $i = 1, 2, 3, 4$ and (x_s, y_s) the heating source location. The Jacobian is based solely on geometry, which

may reduce errors.

$$\frac{\partial r_i}{\partial x_s} = \frac{1}{2} \left((x_i - x_s)^2 + (y_i - y_s)^2 \right)^{-\frac{1}{2}} \left(\frac{\partial}{\partial x_s} (x_i^2 - 2x_i x_s + x_s^2) \right) \quad (4)$$

$$\frac{\partial r_i}{\partial x_s} = \frac{x_s - x_i}{r_i}, \quad \frac{\partial r_i}{\partial y_s} = \frac{y_s - y_i}{r_i} \quad (5)$$

The measurement transition function $b(\bar{X}_t)$ and the Jacobian B_t are then

$$b(\bar{X}_t) = \begin{bmatrix} \sqrt{(x_1 - x_s)^2 + (y_1 - y_s)^2} \\ \sqrt{(x_2 - x_s)^2 + (y_2 - y_s)^2} \\ \sqrt{(x_3 - x_s)^2 + (y_3 - y_s)^2} \\ \sqrt{(x_4 - x_s)^2 + (y_4 - y_s)^2} \end{bmatrix} \quad (6)$$

$$B_t = \begin{bmatrix} \frac{x_s - x_1}{r_1} & \frac{y_s - y_1}{r_1} \\ \frac{x_s - x_2}{r_2} & \frac{y_s - y_2}{r_2} \\ \frac{x_s - x_3}{r_3} & \frac{y_s - y_3}{r_3} \\ \frac{x_s - x_4}{r_4} & \frac{y_s - y_4}{r_4} \end{bmatrix} \quad (7)$$

where t is time in seconds with a time step of 1 second, \bar{r}_i with $i = 1, 2, 3, 4$ is the radius from the sensor to the source if the source is located at (x_s, y_s) , and (x_i, y_i) with $i = 1, 2, 3, 4$ are the locations of the four thermocouples. Based on the flat plate experiment above, sensor noise is assumed be ± 0.045 K and is normally distributed ($\sigma^2 = (0.045/3)^2 = 0.000225$ K²). Since measured temperature is being related to radius, sensor noise must be converted into radius noise. The complication in this conversion arises from the fact that radius is a non-linear function of temperature and time. If a slope ($\partial r/\partial T$) of 0.015 m/K is assumed, the radius noise is ± 0.000675 m and is normally distributed ($\sigma^2 = 5.06 \times 10^{-8}$ m²). The measurement covariance matrix, therefore, is $R = 5.06 \times 10^{-8}$ m² * I_4 .

Ultrasonic Pulse-echo Time of Flight Measurement Model

This model uses ultrasonic pulses to measure the average temperature through the material thickness at each sensor location. In the pulse-echo method, the ultrasonic pulse travels through the

material thickness, reflects off the boundary, and returns to the transducer. The time of flight is [7]

$$G_{ii} = \frac{2L}{v_0} \left(1 + \xi \theta_{avg} \Big|_0^L \right) \quad (8)$$

where L represents the material thickness, v_0 is the speed of sound in the material at a reference temperature, ξ is the ultrasonic time of flight factor which is material dependent, and θ is the change in temperature from the reference temperature. The ultrasonic pulse time of flight measurement model consists of obtaining expected temperatures from COMSOL, computing the average temperature between the transducer and the boundary, and then computing an expected time of flight using equation 8 to form the measurement transition function $b(\bar{X}_t)$ (equation 9). The Jacobian partial derivatives are obtained using time of flight difference when moving the source in the x and y directions independently (equation 10).

$$b(\bar{X}_t) = \begin{bmatrix} \bar{G}_1 \\ \bar{G}_2 \\ \bar{G}_3 \\ \bar{G}_4 \end{bmatrix} \quad (9)$$

$$B_t = \begin{bmatrix} -\frac{\partial \bar{G}_1}{\partial x_1} & -\frac{\partial \bar{G}_1}{\partial y_1} \\ -\frac{\partial \bar{G}_2}{\partial x_2} & -\frac{\partial \bar{G}_2}{\partial y_2} \\ -\frac{\partial \bar{G}_3}{\partial x_3} & -\frac{\partial \bar{G}_3}{\partial y_3} \\ -\frac{\partial \bar{G}_4}{\partial x_4} & -\frac{\partial \bar{G}_4}{\partial y_4} \end{bmatrix} \quad (10)$$

where t is time in seconds with a time step of 1 second, \bar{G}_i with $i = 1, 2, 3, 4$ is the expected ultrasonic pulse time of flight with the heating source at location (x_s, y_s) , and (x_i, y_i) with $i = 1, 2, 3, 4$ are the locations of the four transducers. The Jacobian B_t is constructed using the derivatives with respect to sensor position for convenience since this information can be obtained with one COMSOL simulation. The derivatives are obtained from COMSOL using finite differences by independently varying the x and y positions of all sensors by 0.0001m. Based on the flat plate experiment above, sensor noise is assumed be $\pm 2.3 \times 10^{-10}$ seconds and is normally distributed ($\sigma^2 = 5.88 \times 10^{-21}$ sec²). The measurement covariance matrix, therefore, is $R = 5.88 \times 10^{-21}$ sec² * I_4 .

Radius From Ultrasonic Pulse-echo Time of Flight Measurement Model

In this model, ultrasonic pulse-echo time of flight is measured using four transducers on the non-heated side of the plate. Similar to radius from temperature method, this method converts the measured time of flight to a radius using the COMSOL model as a lookup table. Temperatures in the plate are related to time of flight through equation 8. Equations 3 to 5 develop the geometry behind the measurement transition function $b(\bar{X}_t)$ and the Jacobian B_t which are

$$b(\bar{X}_t) = \begin{bmatrix} \sqrt{(x_1 - x_s)^2 + (y_1 - y_s)^2} \\ \sqrt{(x_2 - x_s)^2 + (y_2 - y_s)^2} \\ \sqrt{(x_3 - x_s)^2 + (y_3 - y_s)^2} \\ \sqrt{(x_4 - x_s)^2 + (y_4 - y_s)^2} \end{bmatrix} \quad (11)$$

$$B_t = \begin{bmatrix} \frac{x_s - x_1}{r_1} & \frac{y_s - y_1}{r_1} \\ \frac{x_s - x_2}{r_2} & \frac{y_s - y_2}{r_2} \\ \frac{x_s - x_3}{r_3} & \frac{y_s - y_3}{r_3} \\ \frac{x_s - x_4}{r_4} & \frac{y_s - y_4}{r_4} \end{bmatrix} \quad (12)$$

where t is time in seconds with a time step of 1 second, \bar{r}_i with $i = 1, 2, 3, 4$ is the radius from the sensor to the source if the source is located at (x_s, y_s) , and (x_i, y_i) with $i = 1, 2, 3, 4$ are the locations of the four thermocouples. Based on the flat plate experiment above, sensor noise is assumed be $\pm 2.3 \times 10^{-10}$ seconds and is normally distributed ($\sigma^2 = 5.88 \times 10^{-21} \text{ sec}^2$). Sensor noise in terms of temperature can be expressed as

$$\theta_{noise} = \frac{G_{noise} v_0}{2L\xi} = 0.84 \text{ K} \quad (13)$$

If the same average slope of 0.015 m/K that was used to relate radius noise to temperature noise in the radius from temperature measurement model, radius noise for the radius from ultrasonic pulse time of flight measurement model is ± 0.0126 m and is normally distributed ($\sigma^2 = 1.76 \times 10^{-5} \text{ m}^2$). The measurement covariance matrix, therefore, is $R_t = 1.76 \times 10^{-5} \text{ m}^2 * I_4$.

Ultrasonic Pulse One-way Time of Flight Measurement Model

Instead of sending an ultrasonic pulse through to a boundary and receiving the echo at the original

transducer, one transducer can transmit the pulse and another transducer can receive the pulse. The time of flight is

$$G_{ij} = \frac{R_{ij}}{v_o} \left(1 + \xi \theta_{avg} |i^j \right) \quad (14)$$

where R_{ij} is the distance between transducers (m). This measurement model consists of obtaining expected temperatures from COMSOL, computing the average temperature between the transducers, and then computing an expected time of flight to form $a(U_t, X_{t-1})$ (equation 15). For the current analysis, the average temperature is based on the line on the plate surface between the two sensors. The Jacobian partial derivatives are obtained using time of flight difference when moving the source in the x and y directions independently (equation 16).

$$b(\bar{X}_t) = \begin{bmatrix} \bar{G}_1 \\ \bar{G}_2 \\ \bar{G}_3 \\ \bar{G}_4 \end{bmatrix} \quad (15)$$

$$B_t = \begin{bmatrix} -\frac{\partial \bar{G}_1}{\partial x_1} & -\frac{\partial \bar{G}_1}{\partial y_1} \\ -\frac{\partial \bar{G}_2}{\partial x_2} & -\frac{\partial \bar{G}_2}{\partial y_2} \\ -\frac{\partial \bar{G}_3}{\partial x_3} & -\frac{\partial \bar{G}_3}{\partial y_3} \\ -\frac{\partial \bar{G}_4}{\partial x_4} & -\frac{\partial \bar{G}_4}{\partial y_4} \end{bmatrix} \quad (16)$$

where t is time in seconds with a time step of 1 second, \bar{G}_i with $i = 1, 2, 3, 4$ is the ultrasonic pulse time of flight with the heating source located at (x_s, y_s) , and (x_i, y_i) with $i = 1, 2, 3, 4$ are the locations of four transducers. The Jacobian B_t is constructed using the derivatives with respect to sensor position for convenience since this information can be obtained with one COMSOL simulation. The derivatives are obtained from COMSOL using finite differences by independently varying the x and y positions of all sensors by 0.0001m. Based on the flat plate experiment above, sensor noise is assumed be $\pm 1.05 \times 10^{-8}$ seconds and is normally distributed ($\sigma^2 = ((1.05 \times 10^{-8})/3)^2 = 1.225 \times 10^{-17} \text{ sec}^2$). The measurement covariance matrix, therefore, is $R = 1.225 \times 10^{-17} \text{ sec}^2 * I_4$.

Ellipse From Ultrasonic Pulse One-way Time of Flight Measurement Model

In this model, a particular ultrasonic pulse time of flight means that the source could be anywhere

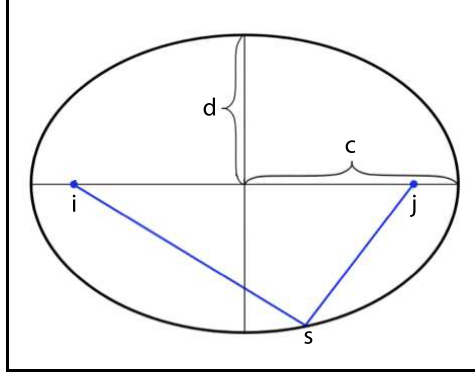


Figure 8. Ellipse properties.

on an elliptical shape around the sensors. Figure 8 illustrates the geometry of an ellipse. The two sensors are assumed to be the focus points for the ellipse. Since the distance between sensors is known, ellipse parameters c and d can be related to each other and the ellipse can be represented with just one parameter c .

$$r_{is} + r_{js} = 2c = \sqrt{r_{ij}^2 + 4d^2} \quad (17)$$

where i and j are sensors and s is heat source.

$$c = \frac{1}{2} \sqrt{r_{ij}^2 + 4d^2} = \frac{r_{is} + r_{js}}{2} \quad (18)$$

$$r_{is} = \sqrt{(x_i - x_s)^2 + (y_i - y_s)^2} \quad (19)$$

$$r_{js} = \sqrt{(x_j - x_s)^2 + (y_j - y_s)^2} \quad (20)$$

$$\frac{\partial c_i}{\partial x_s} = \frac{1}{2} \left[\frac{x_s - x_i}{r_{is}} + \frac{x_s - x_j}{r_{js}} \right] \quad (21)$$

$$\frac{\partial c_i}{\partial y_s} = \frac{1}{2} \left[\frac{y_s - y_i}{r_{is}} + \frac{y_s - y_j}{r_{js}} \right] \quad (22)$$

The parameter c is measured indirectly by first measuring the one-way ultrasonic pulse time of flight. The forward conduction solution is used to get time of flight for a range of c values and interpolated using the spline method to obtain c for the measured time of flight. The c parameter is analogous to radius and is the orthogonal distance from the ultrasonic path between two sensors and the source at s . The measurement transition func-

tion $b(\bar{X}_t)$ and the Jacobian B_t are then

$$b(\bar{X}_t) = \begin{bmatrix} c_1 \\ c_2 \\ c_3 \\ c_4 \end{bmatrix} \quad (23)$$

$$B_t = \begin{bmatrix} \frac{\partial c_1}{\partial x_s} & \frac{\partial c_1}{\partial y_s} \\ \frac{\partial c_2}{\partial x_s} & \frac{\partial c_2}{\partial y_s} \\ \frac{\partial c_3}{\partial x_s} & \frac{\partial c_3}{\partial y_s} \\ \frac{\partial c_4}{\partial x_s} & \frac{\partial c_4}{\partial y_s} \end{bmatrix} \quad (24)$$

(25)

where t is time in seconds with a time step of 1 second, c_i with $i = 1, 2, 3, 4$ is the ellipse parameter if the source is located at (x_s, y_s) . Based on the flat plate experiment above, sensor noise is assumed be $\pm 1.05 \times 10^{-8}$ sec and is normally distributed ($\sigma^2 = 1.22 \times 10^{-17}$ sec²). The sensor noise in terms of temperature can be expressed as

$$\theta_{noise} = \frac{G_{noise} v_0}{L\xi} = 6.09 \text{ K} \quad (26)$$

Using the same average slope of 0.015 m/K that was used to relate radius noise to temperature noise in the radius from temperature measurement model, ellipse noise for the c parameter from ultrasonic pulse time of flight measurement model is $\pm 2.04 \times 10^{-4}$ m and is normally distributed ($\sigma^2 = 4.62 \times 10^{-9}$ m²).

Extended Kalman Filter Convergence Behavior

Extended Kalman filter convergence behavior for all six measurement models are compared in Figures 9 through 12. With the heating source located inside the sensor grid (Figure 9), all measurement models converge to the correct location, however both temperature measurement models exhibit rather noisy convergence. With the heating source located at the edge of the sensor grid (Figure 10), all measurement models once again converge to the correct location and both temperature measurement models and the radius from ultrasonic pulse-echo time of flight measurement model exhibit undesirable convergence behavior. With the heating source located outside of the sensor grid (Figure 11), none of the measurement

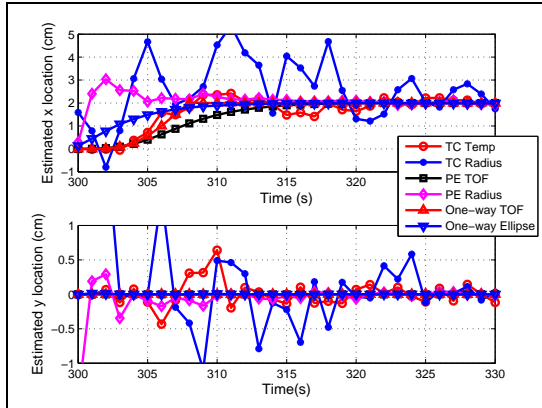


Figure 9. Extended Kalman filter convergence for all six measurement models with source at (2 cm, 0 cm) and initial guess of (0 cm, 0 cm).

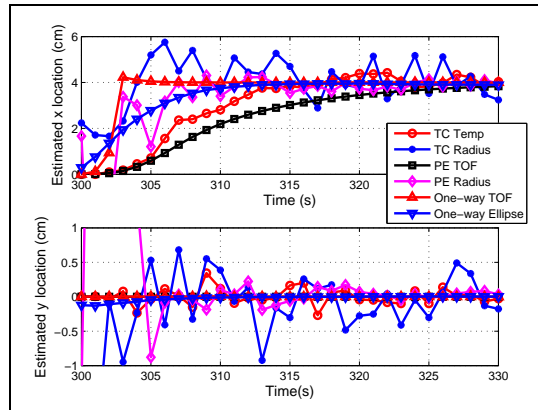


Figure 10. Extended Kalman filter convergence for all six measurement models with source at (4 cm, 0 cm) and initial guess of (0 cm, 0 cm).

models converge to the correct location, however the ellipse from ultrasonic pulse one-way time of flight and radius from ultrasonic pulse-echo time of flight measurement models converge to within 1 cm of the actual location. These examples started with an initial guess of (0 cm, 0 cm) for the heating source location. Figure 12) illustrate the convergence behavior for all six models using an initial guess of (8 cm, 8 cm) for the heating source located at (2 cm, 0 cm). Interestingly, the direct models fail to converge to the correct location in this scenario.

CONCLUSIONS

Results were presented from forward conduction solution development, flat plate experimentation with a known heat source, and parameter identification of heat flux and convection coefficient on the plate. Least squares, extended Kalman filter, and extended information filter inversion methods produced similar results. This finding is significant as future work will add more free parameters (e.g., secondary heating profile) and heat source localization to the inverse procedure. The extended Kalman filter convergence behavior was compared using six measurement models. The one-way ultrasonic pulse measurement model produced the best results when considering accuracy of converged solution, ability to converge to the correct solution

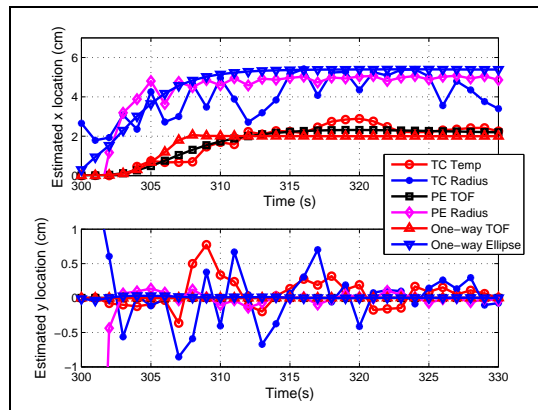


Figure 11. Extended Kalman filter convergence for all six measurement models with source at (6 cm, 0 cm) and initial guess of (0 cm, 0 cm).

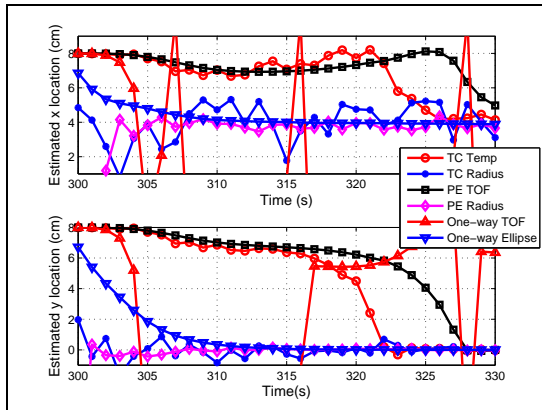


Figure 12. Extended Kalman filter convergence for all six measurement models with source at (2 cm, 0 cm) and initial guess of (8 cm, 8 cm).

given different initial guesses, and smoothness of convergence behavior. Whereas this work had no inputs to the state model, the ability to add inputs to a recursive state estimator (e.g., a Gaussian filter) is anticipated to be more robust for heat source localization and in turn for boundary layer transition localization and characterization.

ACKNOWLEDGEMENTS

The authors would like to acknowledge the financial support from the Brazilian agency Conselho Nacional de Desenvolvimento Científico e Tecnológico (CNPq), the United States Air Force Office of Scientific Research (AFOSR), and the United States Air Force Research Laboratory (AFRL). The authors would also like to acknowledge Dr. Mitch Wilkes, Associate Professor of Electrical Engineering and Associate Professor of Computer Engineering at Vanderbilt University for his assistance in understanding recursive state estimation.

REFERENCES

- [1] H. L. Reed, R. L. Kimmel, S. Schneider, D. Arnal, and W. Saric, "Drag prediction and transition in hypersonic flow," in *Symposium on Sustained Hypersonic Flight, AGARD Conference on Future Aerospace Technology in the Service of the Alliance*, 1997.
- [2] T. J. Horvath, S. A. Berry, and B. R. Hollis, "Boundary layer transition on slender cones in conventional and low disturbance mach 6 wind tunnels," in *32nd AIAA Fluid Dynamics Conference and Exhibit*, 2002.
- [3] V. Kozlov, V. Adamchik, and V. Lipovtsev, "Local heating of an unbounded orthotropic plate through a circular and annular domain," *Journal of Engineering Physics and Thermophysics*, Jan 1989.
- [4] F. P. Incropera and D. P. DeWitt, *Introduction to Heat Transfer*, 4th ed. John Wiley and Sons, 2002.
- [5] S. Thrun, W. Burgard, and D. Fox, *Probabilistic Robotics*. The MIT Press, 2006.
- [6] K. A. Woodbury, "Sequential function specification method using future times for function estimation," in *Inverse Engineering Handbook*, K. A. Woodbury, Ed. CRC Press, 2003.
- [7] M. R. Myers, D. G. Walker, D. E. Yuhas, and M. J. Mutton, "Heat flux determination from ultrasonic pulse measurements," in *proceedings of the International Mechanical Engineering Congress and Exposition*, ser. IMECE2008-69054, Boston, Massachusetts, Nov. 2008.